# Robustness of STDP to spike-timing jitter

Y. Cui, I. Prokin, A. Mendes, H. Berry, L. Venance

## SUPPORTING INFORMATION

## S1 Text - Description of the mathematical model

We describe here the mathematical model used to predict the outcome of STDP stimulations with spike timing jitter. We give here the information necessary to implement the model. Further detail and validation can be found in Cui et al (2016).

**Stimulations**. A STDP protocol consists in a series of $N_{\text{pairings}}$ post- and presynaptic pairs of stimulations. We note $t_{\text{pre}_i}$ the time at which the $i^{\text{th}}$ presynaptic stimulation is delivered and $t_{\text{post}_i}$ the onset time of the $i^{\text{th}}$ postsynaptic step current stimulation, where $i = 1, \dots, N_{\text{pairings}}$. We modeled glutamate concentration in the synaptic cleft, $G(t)$, as a train of exponentially-decaying impulses triggered by presynaptic stimuli at time $t_{\text{pre}_i}$:

$$G(t) = G_{\max} \sum_i \exp\left(-\frac{t - t_{\text{pre}_i}}{\tau_G}\right) \Theta\left(t - t_{\text{pre}_i}\right) \quad \text{(SI1)}$$

where $G_{\max}$ is the peak glutamate concentrations and $\tau_G$ is the glutamate clearance rate. On the postsynaptic side, action currents resulting from postsynaptic stimulations were modeled according to

$$I_{\text{action}}(t) = -\text{DC}_{\max} \sum_i R\left(t, t_{\text{post}_i}, \text{DC}_{\text{dur}}\right) - \text{AP}_{\max} \sum_i \Theta\left(t - \delta - t_{\text{post}_i}\right) \exp\left(\frac{-t + \delta + t_{\text{post}_i}}{\tau_{\text{bAP}}}\right) \quad \text{(SI2)}$$

where the rectangle function $R(t, a, l) = \Theta(t - a) - \Theta(t - a - l)$, $\text{DC}_{\max}$ and $\text{DC}_{\text{dur}}$ are the amplitude and duration of step-current injected by the patch pipette in the postsynaptic soma, $\text{AP}_{\max}$ is the amplitude of the action current producing the bAP; and $\tau_{\text{bAP}}$ is the time scale for bAP decay.

We modeled the electrical response to these stimulations in a postsynaptic element considered as a single isopotential compartment with AMPAR, NMDAR, VSCC and TRPV1 conductances

$$C_{\mathrm{m}}\frac{dV}{dt} = -g_L(V-V_{\mathrm{L}}) - I_{\mathrm{AMPAR}}(V,G(t)) - I_{\mathrm{NMDAR}}(V,G(t)) \\ -I_{\mathrm{VSCC}}(V) - I_{\mathrm{TRPV1}}(V,AEA) - I_{\mathrm{action}}(t) \quad \text{(SI3)}$$

where $V$ is membrane potential; $g_{\mathrm{L}}$ and $V_{\mathrm{L}}$ are leak conductance and reversal potential respectively; $I_{\mathrm{AMPAR}}$, $I_{\mathrm{NMDAR}}$, $I_{\mathrm{VSCC}}$ and $I_{\mathrm{TRPV1}}$ are currents through AMPAR, NMDAR, L-type VSCC (v1.3) and TRPV1, respectively, and AEA stands for anandamide. NMDAR and AMPAR were modeled with two-state kinetic models and 1.0mM $Mg^{2+}$ (Destexhe *et al.,* 1995) whereas the model and parameters for the $Ca_v1.3$ VSCC current was taken from Wolf *et al.* (2005). The TRPV1 current, including its dependence on AEA, was modeled as:

$$I_{TRPV1}(V,AEA) = g_{TRPV1}\cdot V\cdot P_{TRPV1}^{open}(V,AEA) \quad \text{(SI4)}$$

where $g_{TPRV1}$ is the maximal conductance of TRPV1 and the mathematical expression for the $P_{TRPV1}^{open}$ was taken from Matta and Ahern (2007).

**Biochemical signaling**. Free cytosolic calcium is one of the main signaling actors in the model. To model its dynamics, we assumed it can be transferred from/to two main sources: (*i*) extracellular calcium, via the plasma membrane channels of eq. (SI3) above and (*ii*) the endoplasmic reticulum (ER), via the IP3-dependent Calcium-Induced Calcium Release (CICR) system. Hence, the concentration of free cytosolic calcium $C$ was computed according to

$$T_{\mathrm{C}}(C)\frac{dC}{dt} = J_{IP_3R} - J_{\mathrm{SERCA}} + J_{\mathrm{leak}} + J_{\mathrm{NMDAR}} + J_{\mathrm{VSCC}} + J_{\mathrm{TRPV1}} - \frac{C-C_{\mathrm{b}}}{\tau_{C_{\mathrm{b}}}} \quad \text{(SI5)}$$

where the fluxes $J_{\mathrm{IP3R}}, J_{\mathrm{SERCA}}, J_{\mathrm{leak}}$ from and to the ER in the CICR system were taken from the model of De Pittà *et al.* (2009) - see also Cui et al. (2016) and $J_{\mathrm{NMDAR}}, J_{\mathrm{VSCC}}$ and $J_{\mathrm{TRPV1}}$are the calcium fluxes from the plasma membrane channels (eq. SI3), computed as $J_{\mathrm{x}} = \xi_x \cdot I_{\mathrm{x}}$ were the $\xi_x$ are constants, $x \in \{\mathrm{NMDAR,VSCC,TRPV1}\}$. $C_{\mathrm{b}}$ is the basal cytosolic calcium level resulting from equilibration with calcium diffusion out of the cell and $\tau_{C_{\mathrm{b}}}$ is the corresponding time scale. The CICR model also includes the dynamics of the fraction of inactive IP3 (inositol triphosphate) receptor channels (IP3R), $h$

$$\frac{\mathrm{d}h}{\mathrm{d}t} = a_2 d_2 \frac{IP3+d_1}{IP3+d_3}(1-h) - a_2 C h \quad \text{(SI6)}$$

Likewise, the dynamics of $C_{ER}$, the calcium concentration in the endoplasmic reticulum (ER) was given by

$$T_{C_{ER}}\left(C_{ER}\right)\frac{dC_{ER}}{dt} = -\rho_{ER}\left(J_{IP_3R} - J_{SERCA} + J_{leak}\right) \tag{SI7}$$

where $\rho_{ER}$ is the ER to cytoplasm volume ratio. In eq.(SI5) and (SI7), $T_x$ , $x = C$ or $C_{ER,}$ is a time scaling factor accounting for the presence of endogenous calcium buffers and expressed according to

$$T_x\left(x\right) = 1 + \frac{B_T}{K_{dB}\left(1 + x / K_{dB}\right)^2} \tag{SI8}$$

Our model also accounts for the biochemical pathways leading to the production of the endocannabinoids 2-Arachidonoylglycerol (2-AG) and AEA, and their subsequent activation of cannabinoid receptors type-1, $CB_1R$. Principally, the model expresses the kinetics of the following enzymatic reactions: (*i*) synthesis of DAG (diacylglycerol) and IP3 (inositol triphosphate) as a result of glutamate (*G*) binding of metabotropic glutamate receptors (mGluR) and subsequent activation of PLCβ as well as Ca-dependent synthesis by PLCδ, (*ii*) transformation of DAG into 2-AG by DAG Lipase α and (*iii*) synthesis of AEA by calcium-dependent fatty acid amide hydrolase (FAAH). The dynamics of this system was modeled with the following equations:

$$\frac{dIP_3}{dt} = v_\beta \frac{G}{G + K_R + K_P C/\left(C + K_\pi\right)} + \frac{v_\delta}{1 + IP_3/\kappa_d}\frac{C^2}{K_\delta^2 + C^2} - v_{3K} CaMKII * \frac{IP_3^{n_3}}{K_3^{n_3} + IP_3^{n_3}} - r_{5P} IP_3 \tag{SI9}$$

$$\frac{dDAG}{dt} = v_\beta \frac{G}{G + K_R + K_P C/\left(C + K_\pi\right)} + \frac{v_\delta}{1 + IP_3/\kappa_d}\frac{C^2}{K_\delta^2 + C^2} - \frac{r_{DGL} \cdot DAGL \cdot \varphi_{DAGL} \cdot DAG}{DAG + K_{DAGL}} - r_{DAGK} \cdot DAG \tag{SI10}$$

$$\frac{d2AG}{dt} = \frac{r_{DGL} \cdot DAGL \cdot \varphi_{DAGL} \cdot DAG}{DAG + K_{DAGL}} - r_{MAGL} 2AG \tag{SI11}$$

$$\frac{d\varphi_{DAGL}}{dt} = r_k C^{n_c}\left(1 - \varphi_{DAGL}\right) - r_p \varphi_{DAGL} \tag{SI12}$$

$$\frac{dAEA}{dt} = \upsilon_{AT} C - r_{FAAH}\frac{AEA}{K_{FAAH} + AEA} \tag{SI13}$$

where *CaMKII** is the amount of activated (phosphorylated) CaMKII (see below); $\varphi_{DAGL}$ is the fraction of active DAG Lipase α and DAGL its total (activated+not activated) concentration. Eq. (SI9-SI11) account for IP3 degradation by IP3 3-kinase (3K) and inositol polyphosphate 5-phosphatase (5P), while DAG and 2AG are degraded by DAG kinase (DAGK) and monoacylglycerol lipase (MAGL), respectively.

2-AG and AEA are retrograde signaling molecules that are produced in the postsynaptic neuron but diffuse to the presynaptic cell, where they activate $CB_1R$. We modeled $CB_1R$ activation by 2-AG and AEA using a simple three-state kinetic model: open ($x_{\mathrm{CB1R}}$), desensitized ($d_{\mathrm{CB1R}}$) and inactivated ($i_{\mathrm{CB1R}}$):

$$\frac{dx_{CB1R}}{dt} = \alpha_{CB1R} \cdot eCB \cdot i_{CB1R} - \left(\beta_{CB1R} + \gamma_{CB1R}\right) x_{CB1R} \tag{SI14}$$

$$\frac{dd_{CB1R}}{dt} = -\varepsilon_{CB1R} d_{CB1R} + \gamma_{CB1R} x_{CB1R} \tag{SI15}$$

where $eCB = 2\text{-}AG + 0.10\ AEA$ and mass conservation implies $x_{\mathrm{CB1R}} + d_{\mathrm{CB1R}} + i_{\mathrm{CB1R}} = 1$. The open fraction $x_{\mathrm{CB1R}}$ was then used to compute $CB_1R$ activation as

$$y_{\mathrm{CB1R}} = k_{\mathrm{CB1R}} x_{\mathrm{CB1R}} + C_1 \tag{SI16}$$

where $C_1$ is a constant that accounts for the modulation of presynaptic plasticity by other pathways and $k_{\mathrm{CB1R}}$ quantifies the strength of $CB_1R$ activation on presynaptic plasticity.

In our model, $CB_1R$ activation ($y_{\mathrm{CB1R}}$) controls the presynaptic weight $W_{\mathrm{pre}}$ according to the following rule: $W_{\mathrm{pre}}$ decreases for intermediate values of $y_{\mathrm{CB1R}}$, i.e. when $y_{\mathrm{CB1R}}$ is comprised between two tLTD thresholds ($\theta_{\mathrm{LTD}}^{\mathrm{start}} < y_{\mathrm{CB1R}} < \theta_{\mathrm{LTD}}^{\mathrm{stop}}$) whereas $W_{\mathrm{pre}}$ increases when $y_{\mathrm{CB1R}}$ is larger than a tLTP threshold ($y_{\mathrm{CB1R}} > \theta_{\mathrm{LTP}}^{\mathrm{start}}$). Following Cui et al. (2016), we implemented this rule as

$$\Omega(y_{\mathrm{CB1R}}) = \begin{cases} 1 - A_{\mathrm{LTD}} & \text{if } \Theta_{\mathrm{LTD}}^{\mathrm{start}} < y_{\mathrm{CB1R}} < \Theta_{\mathrm{LTD}}^{\mathrm{stop}} \\ 1 + A_{\mathrm{LTP}} & \text{if } \Theta_{\mathrm{LTP}}^{\mathrm{start}} < y_{\mathrm{CB1R}} \\ 1 & \text{otherwise} \end{cases} \tag{SI17}$$

and

$$\frac{\mathrm{d}W_{\mathrm{pre}}}{\mathrm{d}t} = \frac{\Omega(y_{\mathrm{CB1R}}) - W_{\mathrm{pre}}}{\tau_{W_{\mathrm{pre}}}(y_{\mathrm{CB1R}} + C_2)} \quad \text{(SI18)}$$

Here $\Omega$ determines the change of presynaptic plasticity, with a time scale $\tau_{W_{\mathrm{pre}}}$ set to yield rapid changes of $W_{\mathrm{pre}}$ for large $y_{\mathrm{CB1R}}$values and very slow changes at very low $y_{\mathrm{CB1R}}$:

$$\tau_{W_{\mathrm{pre}}}(\mathrm{x}) = \frac{P_1}{P_2^{P_3} + x^{P_3}} + P_4 \quad \text{(SI19)}$$

To account for experimental observation that the presynaptic weight ranges from about 50 to 300%, $W_{\mathrm{pre}}$ was clipped to 3.0 (hard bound).

Postsynaptic plasticity in the model was based on the activation by calcium of calmodulin and CaMKII and the regulation of this system by PKA, calcineurin and protein phosphatase 1 (PP1). The model of Cui et al (2016) for this subsection is based on the model proposed in Graupner & Brunel (2007). In this model the concentration of the calcium/calmodulin complex with four calcium ions bound (CaM) is considered at equilibrium and computed as:

$$CaM = \frac{CaMT}{1 + \sum_{i=1}^{4}(C^i \cdot \prod_{j=5-i}^{4} K_j)} \quad \text{(SI20)}$$

where *CaMT* is the total calmodulin concentration and $K_i$ stands for the equilibrium constant of the binding of the $i^{\mathrm{th}}$ calcium ion to calmodulin. Each CaMKII enzyme consists of two subunits, each of which contains 6 phosphorylation sites, thus defining 14 phosphorylation states per subunit. Denoting $y_i$, $i$=0…13 the concentrations of subunit in phosphorylation state $i$, the model of Graupner & Burnel (2007) expresses their dynamics as:

$$
\begin{aligned}
\frac{dy_1}{dt} &= 6k_6\gamma^2 y_0 - (4k_6\gamma^2 + k_7\gamma + k_{10})y_1 + 2k_{10}\sigma_2^4 \\
\frac{dy_2}{dt} &= (k_7\gamma + k_6\gamma^2)y_1 - (3k_6\gamma^2 + k_7\gamma + 2k_{10})y_2 + k_{10}(y_5 + \sigma_5^7) \\
\frac{dy_3}{dt} &= 2k_6\gamma^2 y_1 - 2(k_7\gamma + k_6\gamma^2 + k_{10})y_3 + k_{10}(\sigma_5^7 + 3y_8) \\
\frac{dy_4}{dt} &= k_6\gamma^2 y_1 - 2(k_7\gamma + k_6\gamma^2 + k_{10})y_4 + k_{10}(y_6 + y_7) \\
\frac{dy_5}{dt} &= k_7\gamma(\sigma_2^3 - y_5) + k_6\gamma^2(y_2 - 2y_5) + k_{10}(2y_9 + y_{10} - 3y_5) \\
\frac{dy_6}{dt} &= k_6\gamma^2(\sigma_2^3 - y_6) + k_7\gamma(2y_4 - 2y_6) + k_{10}(-3y_6 + \sigma_9^{11} + y_{11}) \\
\frac{dy_7}{dt} &= k_6\gamma^2(y_2 + 2y_4 - y_7) + k_7\gamma(y_3 - 2y_7) + k_{10}(-3y_7 + \sigma_9^{11} + y_{11}) \\
\frac{dy_8}{dt} &= k_6\gamma^2 y_3 - 3k_7\gamma y_8 + k_{10}(y_{10} - 3y_8) \\
\frac{dy_9}{dt} &= k_7\gamma(\sigma_5^7 - y_9) + k_6\gamma^2(y_5 - y_9) + k_{10}(-4y_9 + 2y_{12}) \\
\frac{dy_{10}}{dt} &= k_6\gamma^2 y_5 + k_6\gamma^2 y_6 + k_7\gamma(y_7 + 3y_8 - 2y_{10}) + k_{10}(2y_{12} - 4y_{10}) \\
\frac{dy_{11}}{dt} &= k_7\gamma(y_6 - 2y_{11}) + k_6\gamma^2 y_7 + k_{10}(y_{12} - 4y_{11}) \\
\frac{dy_{12}}{dt} &= k_6\gamma^2 y_9 + k_7\gamma(2\sigma_9^{11} - y_9 - y_{12}) + k_{10}(6y_{13} - 5y_{12}) \\
\frac{dy_{13}}{dt} &= k_7\gamma y_{12} - 6k_{10}y_{13}
\end{aligned}
\qquad \text{(SI21)}
$$

where $\sigma_i^j = \sum_{k=i}^{j} y_k$ and mass conservation implies $y_0 = 2CaMKII_0 - \sigma_1^{13}$, where $CaMKII_0$ is the total CaMKII concentration. In eq. (SI21) above the probabilities that CaM binds to phosphorylated ($\gamma$) and dephosphorylated ($\gamma^*$) subunit of CaMKII are computed as $\gamma = CaM/(CaM + K_5)$ and $\gamma^* = CaM/(CaM + K_9)$. Moreover, the rate of subunit dephosphorylation ($k_{10}$) is given by $k_{10} = k_{12}PP1/(K_M + CaMKII^*)$ where $K_M$ is a constant, $PP1$ is the concentration of PP1. $CaMKII^*$ is the total concentration of phosphorylated subunits of CaMKII computed accross all possible states of phosphorylation $CaMKII^* = \sum_{i=0}^{13} m_i y_i$ where $m_i$ is the number of the phosphorylated subunits of CaMKII in state $i$ and $y_i$.

Finally, the model of Graupner & Brunel (2007) assumes that, in addition to calcineurin (CaN), PKA activity depends on CaM according to a Hill-function activation:

$$
\nu_x(CaM) = k_x^0 + \frac{k_x}{1 + (K_x/CaM)^{n_x}} \qquad \text{(SI22)}
$$

where $x = CaN$ or $PKA$, The interaction between PP1 and I1 is then described as:

$$
\begin{aligned}
\frac{dI1}{dt} &= \frac{dPP1}{dt} - \nu_{CaN} I1 + \nu_{PKA} I1_0 \\
\frac{dPP1}{dt} &= -k_{13} I1 \cdot PP1 + k_{-13}(PP1_0 - PP1)
\end{aligned}
\qquad \text{(SI23)}
$$

where $PP1_0$ and $I1_0$ are total PP1 and I1 concentrations, respectively.

In agreement with Cui et al. (2016) and Graupner & Brunel (2007), we assumed that postsynaptic plasticity is directly proportional to the calcium-dependent activation of CaMKII and set:

$$W_{\text{post}} = 1 + 3.5\frac{CaMKII^*}{CaMKII^*_{\text{max}}} \quad \text{(SI24)}$$

where $CaMKII^*_{\text{max}}$ is the maximal concentration of activate (phosphorylated).

Finally, the total synaptic weight was taken as the product of the presynaptic and the postsynaptic contributions above:

$$W_{\text{total}} = W_{\text{pre}}W_{\text{post}} \quad \text{(SI25)}$$

**Model implementation and numerics.** Our mathematical model comprises 36 ordinary differential equations and close to 150 parameters, among which more than one half is constrained by experimental data. Initial conditions were set to the steady-state of each variable in the absence of stimulation. Numerical solution was obtained with the LSODA solver from the ODEPACK fortran77 library with absolute and relative tolerances both equal to $10^{-7}$. Initial conditions were set to the steady-state of each variable in the absence of stimulation. Numerical integration proceeded until the synaptic weights reach stable values (typically observed around t ≈ 5min after the stimulation protocol). We used the final values of the pre- and postsynaptic weights to compute the total synaptic weight change due to the stimulations. Importantly, with the exception of the stimulation protocols, *we have used the exact same equations and parameter values as in* Cui et al. (2016). The list of parameters and their estimated values is given in S2 Table. The current study employs stochastic simulations since the stimulation protocol is stochastic (while the rest of the model is deterministic). Therefore, the model was calibrated using experimental data from deterministic stimulation

protocols (Cui et al., 2016) and we tested here whether it can make successful predictions when we applied stochastic stimulation protocols, for which the model was not calibrated. The results are thus averages over $N_{trials}$ realizations. $N_{trials}$ was varied from 30 to 500 depending on the smoothness of the averaged curves and values of SEM, but $N_{trials}$=50 in most of the simulations. The computer code of the model is available online from https://github.com/iprokin/Cx-Str-STDP and https://senselab.med.yale.edu/modeldb/ShowModel.cshtml?model=187605.

# S2 Table – Parameter values

## A. Intracellular dynamics

| Description | Name | Values | Units | Reference |
|---|---|---|---|---|
| $I_{NMDAR}$ to Ca flow conversion | $\xi_{NMDAR}$ | 98 | µM/pCol | set to match Ca2+ amplitudes in [1] |
| $I_{VSCC}$ to Ca flow conversion | $\xi_{VSCC}$ | 140 | µM/pCol | set to match Ca2+ amplitudes in [2] |
| $I_{TRPV1}$ to Ca flow conversion | $\xi_{TRPV1}$ | 290 | µM/pCol | set to match Ca2+ amplitudes in [1] |
| Total endogenous Ca buffer | $B_T$ | 4.5 | µM | Estimated from our experimental data |
| Basal cytoplasmic [Ca] | $C_b$ | 0.1 | µM | [1,3] |
| Time scale for Ca exit | $\tau_{Cb}$ | 0.007 | s | Idem |
| Endogenous Ca buffer affinity | $K_{dB}$ | 0.5 | µM | [3,4] |
| ER-to-cytosol volume ratio | $\rho_{ER}$ | 0.3 | - | Adapted from [4] |
| IP3R binding rate (inactivation) | $a_2$ | 0.5 | µM/s | Idem |
| Maximal SERCA pump rate | $v_{ER}$ | 8 | µM/s | Idem |
| IP3R affinity for IP3 | $d_3$ | 0.9434 | µM | [5] |
| Maximal IP3R rate | $r_C$ | 4 | 1/s | Adapted from [5] |
| Basal [Ca] in the ER | $Ca_{ER,b}$ | 65 | µM | [6] |
| Ca leak from the ER | $r_l$ | 0.1 | 1/s | [5] |
| IP3R affinity for Ca | $d_5$ | 0.12 | µM | Adapted from [5] |
| IP3R dissociation constant | $d_2$ | 3.049 | µM | Idem |
| SERCA pump affinity for Ca | $K_{ER}$ | 0.05 | µM | [5] |
| IP3R affinity for IP3 | $d_1$ | 0.13 | µM | Idem |
| PLCδ product inhibition | $\kappa_d$ | 1.5 | µM | Idem |
| PLCδ Ca-activation | $K_\delta$ | 0.1 | µM | Idem |
| 5P-IP maximal rate | $r_{5P}$ | 0.2 | 1/s | Adapted from [5] |
| PI3K maximal rate | $v_{3K}$ | 0.001 | µM/s | Idem |
| PI3K Ca-activation constant | $K_D$ | 1.5 | µM | Idem |
| PLCδ maximal rate | $v_\delta$ | 0.02 | µM/s | [5] |
| PI3K affinity for IP3 | $K_3$ | 1 | µM | Idem |
| Glutamate affinity to mGluR | $K_R$ | 1.3 | µM | Idem |
| regulation by PLCβ termination | $K_P$ | 10 | µM | Idem |
| PLCβ maximal rate | $v_\beta$ | 0.8 | µM/s | Adapted from [5] |
| PKC Ca-activation constant | $K_\pi$ | 0.6 | µM | [5] |
| Total CaMKIIα concentration | $CaMKII_0$ | 16.6 | µM | [7] |
| Total Calmodulin concentration | $CaMT$ | 0.07085 | µM | Adapted from [7] |
| PKA Hill number | $n_{PKA}$ | 3 | - | Idem |

Referenced articles: [1] Sabatini, B.L., Oertner, T.O. and Svoboda, K. (2002) *Neuron* 33(3):439-452 [2] Carter, A.G. and Sabatini, B.L. (2004) *Neuron* 44(3):483-493 [3] Jackson, M.B. and Redman, S.J. (2003) *J Neurosci* 23:1612–1621 [4] Nägerl, U.V. *et al.* (2000) *Biophys J* 79: 3009–3018 [5] De Pittà M. *et al.* (2009) *J Biol Phys* 35:383-411 [6] Solovyova, N. *et al.* (2002) *EMBO J* 21:622-630 [7] Graupner, M. and Brunel, N. (2007) *PLoS Comput Biol* 3:e221.

## B. Electrophysiology

| Description | Name | Values | Units | Reference |
|---|---|---|---|---|
| TRPV1R max. conductance | $g_{TRPV1}$ | 0.0003 | nS | Estimated from our experimental data |
| Permeability of L-type VSCC | $p_{VSCC}$ | 0.00000102 | µM/s | Value of [1], scaled to ~5,000 spines, radius 1 µm |
| AMPAR maximal conductance | $g_{AMPAR}$ | 5.1 | nS | Estimated from our experimental data |
| AMPAR closing rate constant | $\beta_{AMPAR}$ | 190 | 1/s | Adapted from [2] |
| AMPAR opening rate constant | $\alpha_{AMPAR}$ | 1.02 | 1/(µM.s) | Idem |
| NMDAR maximal conductance | $g_{NMDAR}$ | 1.53 | nS | Estimated from our experimental data |
| Magnesium concentration | $Mg$ | 1 | mM | Directly measured in our experiments |
| NMDAR opening rate constant | $\alpha_{NMDAR}$ | 0.072 | 1/(µM.s) | Set to emulate the experimental kinetics of NMDAR-transported Ca in [3] |
| NMDAR closing rate constant | $\beta_{NMDAR}$ | 100 | 1/s | Idem |
| Resting membrane potential | $V_L$ | -70 | mV | Directly measured in our experiments |
| Leak conductance | $g_L$ | 10 | nS | Idem |
| Membrane capacitance | $C_m$ | 0.1 | nF | Idem |
| Extracellular Ca2+ concentration | $Ca_{out}$ | 5000 | µM | [1] |
| Duration of depolarization step | $DC_{dur}$ | 0.03 | s | From the experimental stimulation protocol |
| Amplitude of depolarization step | $DC_{\max}$ | 495 | pA | Idem |
| Amplitude of action current | $AP_{\max}$ | 7020 | pA | [4] |
| Time constant of action current | $\tau_{bAP}$ | 0.001 | s | Idem |
| Glutamate peak concentration in the cleft | $G_{\max}$ | 2000 | µM | Estimated from our experimental data |
| Glutamate decay time constant in the cleft | $\tau_G$ | 0.005 | s | Estimated from our experimental data |
| Delay to bAP outset | $\delta$ | 0.015 | s | From the experimental stimulation protocol |
| Stimulation frequency | $F_{\text{pairings}}$ | 1 | Hz | From the experimental stimulation protocol |

Referenced articles: [1] Wolf, J.A. *et al.* (2005) *J Neurosci* 25(40):9080-9095 [2] Destexhe, A., Mainen, Z., and Sejnowski, T. (1994) *J Comput Neurosci* 1:195-230 [3] Sabatini, B.L., Oertner, T.O. and Svoboda, K. (2002) *Neuron* 33(3):439-452 [4] Fino, E., *et al*. (2010) *J Physiol* 588:3045-3062.

## C. Endocannabinoid dynamics

| Description | Name | Values | Units | Reference |
|---|---|---|---|---|
| Scaling factor for endocannabinoid contribution to plasticity | $k_{CB1R}$ | 3000 | 1/µM | Estimated from our experimental data |
| presynaptic plasticity time scale | $P_1$ | 1e-9 | s | Set to yield rapid / slow changes of Wpre for high / low 2-AG values, respectively |
| presynaptic plasticity time scale | $P_2$ | 1e-5 | - | Idem |
| presynaptic plasticity time scale | $P_3$ | 7 | - | Idem |
| presynaptic plasticity time scale | $P_4$ | 2 | s | Idem |
| The lower limit of LTD induction | $\theta_{LTD}^{start}$ | 0.027 | - | Estimated from our experimental data |
| The upper limit of LTD induction | $\theta_{LTD}^{stop}$ | 0.047 | - | Idem |
| The constant determining the rate of LTD induction | $A_{LTD}$ | 0.65 | - | Idem |
| The lower limit of LTP induction | $\theta_{LTP}^{start}$ | 0.087 | - | Idem |
| The constant determining the rate of LTP induction | $A_{LTP}$ | 10.8 | - | Idem |
| CB1R opening rate constant | $\alpha_{CB1R}$ | 0.2402 | 1/(µM.s) | Idem |
| CB1R closing rate constant | $\beta_{CB1R}$ | 11.072 | 1/s | Idem |
| CB1R desensitization rate constant | $\gamma_{CB1R}$ | 416.38 | 1/s | Idem |
| CB1R closing rate constant | $\varepsilon_{CB1R}$ | 0.047796 | 1/s | Idem |
| DAGL α affinity for DAG | $K_{DAGL}$ | 30 | µM | [1] |
| Maximal rate of MAG lipase | $r_{MAGL}$ | 0.5 | µM/s | Set for rapid turnover dynamics. |
| Maximal DAGL α rate | $r_{DGL}$ | 20000 | µM/s | Idem |
| DAG kinase rate | $r_{DAGK}$ | 2 | $s^{-1}$ | Idem |
| Hill number for DAGL activation by Ca | $n_c$ | 6 | - | Estimated from our experimental data |
| DAGL dephosphorylation rate | $r_P$ | 380 | $s^{-1}$ | Idem |
| DAGL phosphorylation rate | $r_K$ | 50 | $\mu M^{-1}.s^{-1}$ | Idem |
| Total DAGL concentration | $DAGL$ | 1 | µM | Idem |
| N-acetyltransferase activity | $v_{AT}$ | 0.2 | 1/s | Idem |
| FAAH Michaelis-Menten constant | $K_{FAAH}$ | 1 | µM | [1] |
| FAAH enzyme activity | $r_{FAAH}$ | 4 | µM/s | Estimated from our experimental data |

Referenced articles: [1] Okamoto, Y. et *al.* (2004) *J Biol Chem* 279:5298-5305.

## S3 Text – Mechanisms of STDP expression in the model

We give here an overview of the mechanisms that give rise to the expression of eCB-tLTP, eCB-tLTD and NMDAR-tLTP in our mathematical model. All the examples given here concern regular (deterministic) STDP protocols with constant IPI and spike timings.

Our model combines the two signaling pathways involved in cortico-striatal STDP: a first signaling pathway leading from NMDAR to calmodulin and CaMKII with a second that couples mGluR and cytosolic calcium to eCB production and the resulting activation of $CB_1R$ (see Fig. 1f1). In the model, we assume that the total synaptic weight ($W_{\mathrm{Total}}$) is the product of presynaptic ($W_{\mathrm{Pre}}$) and postsynaptic ($W_{\mathrm{Post}}$) weights (see Supporting Information S1).

On the postsynaptic side, $W_{\mathrm{Post}}$ is proportional to the amount of CaMKII activated by the NMDAR pathway. CaMKII in our model forms a bistable system that settles at long times either on a "DOWN" state where CaMKII is mostly inactive (no plasticity) or on an "UP" state characterized by high levels of activated CaMKII (Fig. 2b1) (NMDAR-tLTP). In the example of the figure, the time needed for CaMKII dephosphorylation is larger than the interval between two successive pairings, so activated CaMKII accumulates with the number of pairings during the protocol. For a transition from the UP to the DOWN state to occur, the amount of activated CaMKII needs to overcome the separatrix between the two states. The separatrix is reached in the example of *Supplementary Figure S2* (in Supporting Information S4 below) for circa 50-60 post-pre pairings (with $\Delta t_{STDP}$ =-15 ms) (Fig. S2a1). Therefore, in the conditions of Figure S2 (short post-pre pairings), $W_{\mathrm{Post}}$ converges to the UP state (potentiation) only when the STDP protocol comprises > 50 post-pre pairings. With pre-post pairings, the calcium released after each pairing activates less calmodulin than with post-pre protocols. As a result, activated CaMKII never reaches the threshold for the UP state (Fig. S2a2). To summarize, the model successfully reproduces the experimental observations that (*i*) NMDAR-dependent tLTP emerges after 50-75 short post-pre pairings and (*ii*) no NMDAR-dependent LTP is obtained with pre-post pairings (Cui et al., 2016).

When a stimulation protocol composed of 100 pairings is applied, the evolution of the amplitude of the triggered calcium peaks is biphasic (Fig. S2c): it increases up to 10-20 pairings and decreases afterwards to settle to constant amplitude after circa 50 pairings. For the first 10-20 stimulations, the iterated activation of mGluRs leads to the accumulation of IP3, which contributes an extra influx of calcium from the endoplasmic reticulum through calcium-induced calcium release. This extra-boost of cytoplasmic calcium however vanishes when the number of pairings increases further because the concentration of calcium in the ER

decreases. This decay ER calcium eventually compensates the effect of IP3 accumulation on the calcium-induced calcium release, thus stabilizing the amplitude of the calcium peaks for $N_{pairings}$>50. Moreover, since the width of the postsynaptic calcium peak in the model is larger with post-pre than pre-post pairings (Fig S2b), the fraction of calcium-activated DAGLα is much larger for post-pre pairings. As a result, the amplitude of eCB peaks and, ultimately, the amplitude of the fraction of activated $CB_1R$ ($y_{CB1R}$), show a more pronounced biphasic profile (Fig S2d). The biphasic trend is further amplified at the level of $CB_1R$ activation because of $CB_1R$ receptor desensitization that amplifies the decay above 20 pairings (Fig S2d). The amplitude of the $y_{CB1R}$ peaks increases sharply for the first 10-20 pairings, and progressively decays afterwards to converge to constant amplitude. As show in the figure, $y_{CB1R}$ reaches large values only for short post-pre pairings ($\Delta t_{STDP}$ around -15 ms) while even short pre-post pairings ($0< \Delta t_{STDP} <10$ ms) do not give rise to such large amplitude peaks.

The dynamics of the level of $y_{CB1R}$ is responsible for the emergence of eCB-dependent plasticity in the model. Indeed, in the model, $W_{Pre}$ depends on $y_{CB1R}$ with the piecewise constant function shown in Figure S2e and its 3 thresholds $\Theta_{LTD}^{start}$, $\Theta_{LTD}^{stop}$ and $\Theta_{LTP}^{start}$: if $y_{CB1R}$ reaches moderate amounts, i.e. lies within $[\Theta_{LTD}^{start}, \Theta_{LTD}^{stop}]$, $W_{Pre}$ decays (thus emulating eCB-tLTD); whereas $W_{Pre}$ increases (eCB-tLTP) if $y_{CB1R} > \Theta_{LTP}^{start}$ (see the dashed lines in Fig. S2d and summary in Fig. S2e). With short pre-post pairings ($10 < \Delta t_{STDP} <40$ ms), $y_{CB1R}$ enters the LTD range during most of protocol so each pairing contributes a increment of $W_{Pre}$ reduction. Since $W_{Post}$ is not changed with positive, pre-post pairings (Fig. S2a2), pre-post pairings globally lead to a progressive reduction of $W_{Total}$, i.e. the expression of eCB-tLTP. The situation is different for post-pre pairings. The amplitude of $y_{CB1R}$ peaks overcomes $\Theta_{LTP}^{start}$ for ≈ 5 to 30 post-pre-pairings with short $\Delta t_{STDP}$ (around -15 ms), yielding a strong increase of $W_{Pre}$. Given that more that 50 post-pre pairings are needed to alter $W_{Post}$ (Fig. S2a1), the expansion of $W_{Pre}$ leads to eCB-tLTP. However, when $N_{pairings} > 30$ post-pre pairings, $y_{CB1R}$ amplitude gets back below $\Theta_{LTP}^{start}$ so that the initial increase of $W_{Pre}$ does not continue beyond 30 post-pre pairings. This property of the model dynamics emulated the experimental observation that eCB-tLTP disappears when the number of pairings becomes larger than 25-30.

Therefore, the mechanisms that lead to the expression of eCB-dependent plasticity with regular deterministic stimulation protocols in our model can be summarized as follow. eCB-tLTD requires moderate levels of $CB_1R$ activation that are reached with pre-post but not pre-post pairings. The expression of eCB-tLTP however demands larger amounts of $CB_1R$

activation, which are reached only during the first 5-30 post-pre pairings, where every component of the system contributes maximally to $CB_1R$ activation. When the number of post-pre pairings becomes larger than 30, calcium efflux from the internal calcium stores decreases and $CB_1R$ desensitization increases: $CB_1R$ activation becomes insufficient to support such high values of $CB_1R$ activation, so eCB-tLTP vanishes.

# S4 Figure – Supplementary Figures

Figure S1

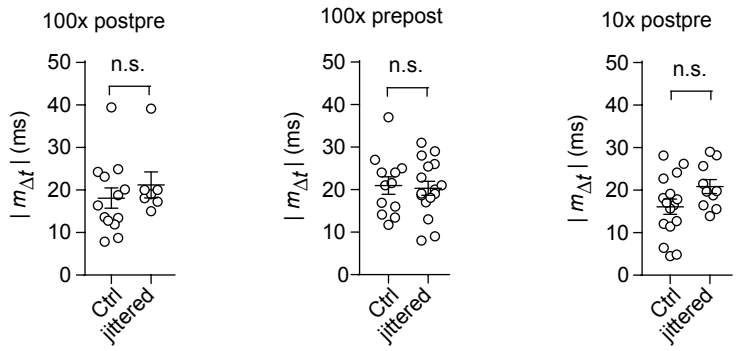


**Supplementary Figure 1: $m_{\Delta t}$ values were not significantly different among STDP paradigms**. $m_{\Delta t}$ were not significantly different in control and jittered conditions for 100 post-pre, 100 pre-post and 10 post-pre pairings (empty circles: individual neurons; black circle: average). Error bars represent the SEM. ns: not significant.

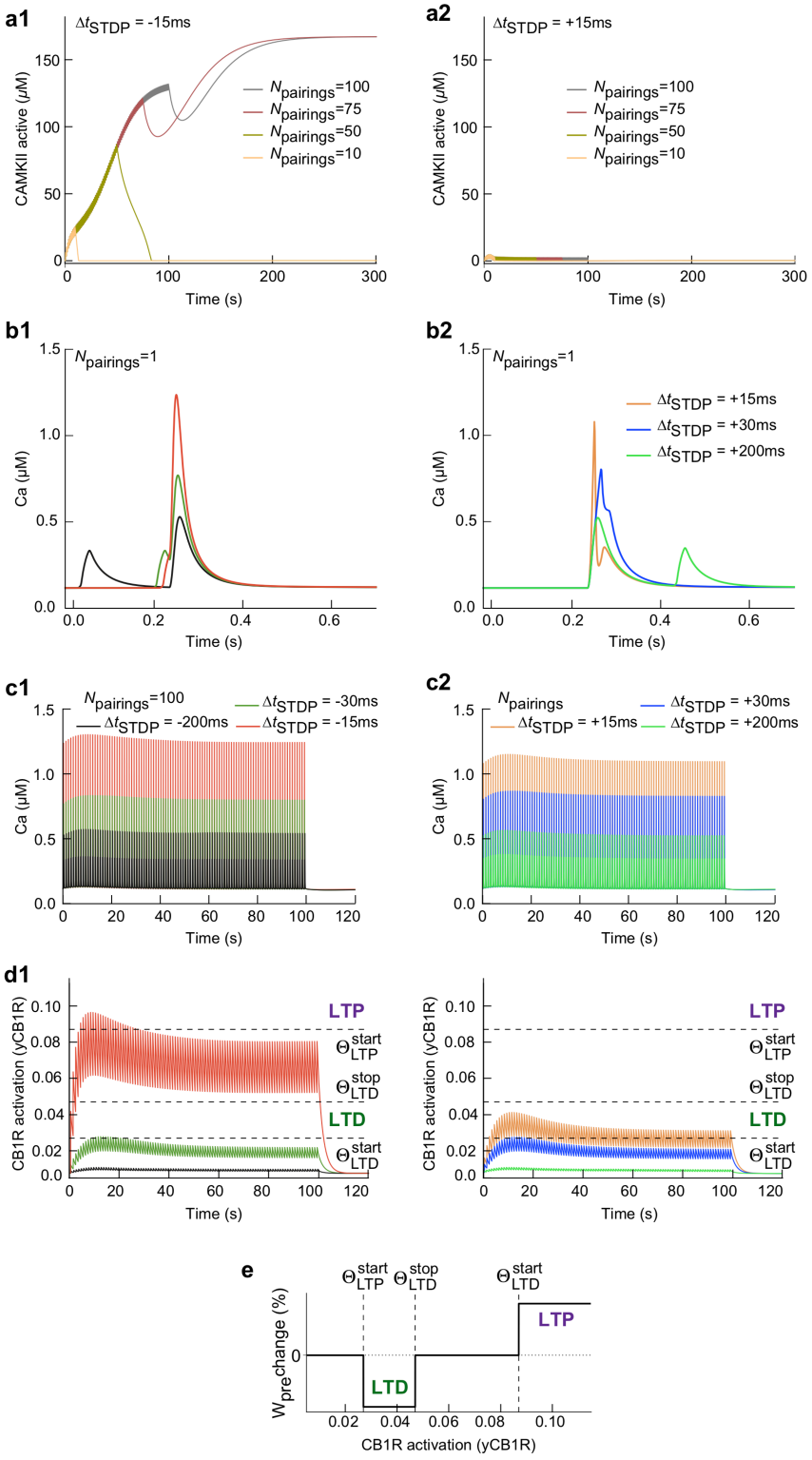


**Supplementary Figure 2**: **Mechanisms of STDP expression in the model with deterministic stimulation protocols**.

(**a**) Changes in the amount of active CaMKII starting from the down (non-activated) state. The number of pairings, $N_{\text{pairings}}$, is indicated for spike-timing $\Delta t_{STDP}$ = -15 (**a1**) or + 15 (**a2**) ms. (**b**) Intracellular calcium changes for the first pairing in post-pre (**b1**) or pre-post (**b2**) pairing protocols. (**c**) Predicted dynamics of the cytoplasmic calcium for 100 post-pre (**c1**) or 100 pre-post pairings (**c2**) and corresponding activation of CB1R, $y_{\text{CB1R}}$ (**d**). The spike-timing $\Delta t_{STDP}$ for each curve is indicated in the legend. (**e**) The presynaptic weight $W_{\text{Pre}}$ changes as a function of $y_{\text{CB1R}}$: it decreases (LTD) when $y_{\text{CB1R}}$ reaches intermediate values and it increases (LTP) if $y_{\text{CB1R}}$ overcomes the LTP threshold. The corresponding thresholds are reported in D as dashed lines. For all the simulations shown, the stimulation protocols were deterministic (regular) with a frequency of 1Hz.

## SUPPLEMENTARY REFERENCES


Cui Y, Prokin I, Xu H, Delord B, Genet S, Venance L, Berry H. (2016) Endocannabinoid dynamics gate spike-timing dependent depression and potentiation. eLife **5**:1–32.

De Pittà M, Goldberg M, Volman V, Berry H, Ben-Jacob E. (2009) Glutamate regulation of calcium and IP3 oscillating and pulsating dynamics in astrocytes. J Biol Phys **35**:383–411.

Destexhe A, Mainen ZF, Sejnowski TJ (1995) Fast kinetic models for simulating AMPA, NMDA, GABA a and GABA B receptors. The Neurobiology of Computation:9–14.

Graupner M, Brunel N (2007) STDP in a bistable synapse model based on CaMKII and associated signaling pathways. PLoS Comput Biol **3**:e221.

Matta JA, Ahern GP (2007) Voltage is a partial activator of rat thermosensitive TRP channels. J Physiol **585**:469–482.

Wolf JA, Moyer JT, Lazarewicz MT, Contreras D, Benoit-Marand M, O'Donnell P, Finkel LH (2005) NMDA/AMPA ratio impacts state transitions and entrainment to oscillations in a computational model of the nucleus accumbens medium spiny projection neuron. J Neurosci **25**:9080–9095.